scientific reports

Check for updates

OPEN

Mitochondrial electron transport chain is essential for acute inflammatory stress responses in mouse fibroblasts

Marie M. Mühlon[1], Christina Schenkl[1,2], Lukas Harder[3,4,5], Luca Giordano[6], Julian M. Voll[1], Christian Franke[3,4,5], Diana Dudziak[2,7,8,9,10], Torsten Doenst[1], Ralf A. Claus[11,12] & Marten Szibor[1,9,13]✉

Fibroblasts are linked to stress responses in a broad number of diseases. Here, we used immortalized mouse embryonic fibroblasts (iMEFs) to elucidate their signaling behavior in response to proinflammatory lipopolysaccharides (LPS) and angiotensin II (Ang-II). To test for the role of the mitochondrial electron transport chain (ETC), iMEFs were cultured in glucose- and galactose-containing media promoting glycolysis and mitochondrial oxidative phosphorylation, respectively. In addition, we used alternative oxidase (AOX), a ubiquinol oxidoreductase that serves as a naturally evolved rescue mechanism in case of ETC disruption. We found that within 24 h of treatment, LPS upregulated a number of proinflammatory genes, namely *Tlr4*, *Il6*, *Tgfb1*, *Nlrp3*, *Casp1*, and *Il1b*; largely, the effect was more pronounced in galactose-containing media and attenuated by AOX. The increase in transcripts resulted partly in elevated cytokine secretion. Twenty-four hours of Ang-II treatment also induced these genes, albeit to a lesser degree and less sensitive to AOX. Cellular oxygen consumption rates (OCRs) were higher in galactose media but remained unaffected by either stimulus. Our results suggest that fibroblasts undergo a similar proinflammatory phenotypic shift in response to different stressors. This response is shaped by ETC activity, which, surprisingly, is not reflected in altered OCRs.

Keywords Mouse, Fibroblasts, Inflammatory response, Mitochondria, Electron transport chain, Alternative oxidase

Organ-resident fibroblasts emerged as central signaling hubs in tissue homeostasis and repair, health and disease. Under physiological conditions, fibroblasts ensure tissue integrity and organ function by facilitating the production and remodeling of the extracellular matrix (ECM). Upon stress, e.g., injury, fibroblasts become activated, start to proliferate and undergo a phenotypic shift to myofibroblasts, a contractile cell population expressing proinflammatory cytokines, chemokines, growth factors and ECM-related proteins, eventually orchestrating fibrosis[1–4].

Specific stimuli and fibroblasts' response mechanisms differ depending on the organ and cellular context. In the heart, for example, persisting pressure overload is a strong trigger for fibroblast activation. This activation is

[1]Department of Cardiothoracic Surgery, Jena University Hospital, Am Klinikum 1, 07747 Jena, Germany. [2]Comprehensive Cancer Center Central Germany – Jena site, Jena University Hospital, Bachstraße 18, 07743 Jena, Germany. [3]Faculty of Physics and Astronomy, Institute for Applied Optics and Biophysics, Friedrich Schiller University Jena, Helmholtzweg 4, 07743 Jena, Germany. [4]Jena Center for Soft Matter, Friedrich Schiller University Jena, Jena, Germany. [5]Abbe Center of Photonics, Friedrich Schiller University Jena, Jena, Germany. [6]Universities of Giessen and Marburg Lung Center (UGMLC), Member of the German Center for Lung Research (DZL), Cardio-Pulmonary Institute (CPI), Justus-Liebig-University, Aulweg 130, 35392 Giessen, Germany. [7]Institute of Immunology, Jena University Hospital, Leutragraben 3, 07743 Jena, Germany. [8]Cluster of Excellence Balance of the Microverse, Friedrich Schiller University Jena, Jena, Germany. [9]Center for Sepsis Control and Care (CSCC), Jena University Hospital, Am Klinikum 1, 07747 Jena, Germany. [10]Core Facility Cytometry, Jena University Hospital, Leutragraben 3, 07743 Jena, Germany. [11]Department of Anesthesiology and Intensive Care Medicine, Jena University Hospital, Am Klinikum 1, 07747 Jena, Germany. [12]Center for Molecular Biomedicine, Jena University Hospital, Hans-Knöll-Str. 2, 07745 Jena, Germany. [13]Faculty of Medicine and Health Technology, Tampere University, FI-33014 Tampere, Finland. ✉email: Marten.Szibor@tuni.fi

driven by mechanical stress but also by neurohumoral factors such as angiotensin II (Ang-II). Mechanical stress induces the release of damage-associated molecular patterns (DAMPs) from injured or dying cardiomyocytes. Fibroblasts respond to DAMPs *via* their pattern-recognition receptors[5,6]. Conversely, Ang-II is a primary driver of cardiac hypertrophy and activates the TGF-β1-Smad signaling pathway[5,7]. In case of sustained activation of cardiac fibroblasts, for instance in the course of chronic pressure overload, excessive deposition of ECM proteins and increased tissue stiffness trap the heart in a vicious cycle that reinforces fibrotic signaling and maladaptive remodeling[5,8].

Notably, fibroblasts constitute a heterogeneous cell population that plays a central role in cardiac remodeling and development and exhibits remarkable plasticity in terms of phenotype and function. For instance, a subset of cardiac fibroblasts responds to chronic pressure overload with the activation of NF-κB signaling, which leads to enhanced C-C motif chemokine ligand 2 expression (CCL2, *aka* monocyte chemoattractant protein-1, MCP1), a potent chemoattractant for inflammatory monocytes[9,10]. Upon differentiation in heart tissue, inflammatory macrophages further enhance fibroblast activation through the secretion of cytokines such as IL-1β, growth factors, and ECM proteins. Chronic pressure overload thus creates an environment of sterile inflammation, formed and reinforced by close interaction between immune cells and fibroblasts, which is crucial in the etiology of heart failure[11,12].

The essential role of cardiac fibroblasts in inflammatory host response is further substantiated by their function in local and systemic inflammation, such as in sepsis. Septic cardiomyopathy is a frequent consequence of sepsis and, as a complication, is associated with a poor prognosis[13–15]. As in the case of pressure overload, the predominant clinical symptom in septic cardiomyopathy is contractile dysfunction. For the development of contractile dysfunction, however, infection is not a prerequisite, as endotoxemia can cause a similarly detrimental phenotype[16,17].

From the aforementioned, it appears that aberrant inflammatory signaling constitutes a canonical stress response in the heart to seemingly distinct stressors. A better understanding of molecular mechanisms that integrate different signals into a canonical signaling pathway may help to prevent maladaptive consequences to stress. One unifying element across different stressors appears to be an involvement of the mitochondrial electron transport chain (ETC). In fact, ETC dysfunction has been suspected in the course of pressure-induced heart failure[18–21] and sepsis-induced cardiomyopathy[22,23]. Given the clinical presentation, much attention has been given to cardiomyocytes; however, noncontractile cells, including fibroblasts, likely play a central role in the development of organ dysfunction.

Here, we set out to investigate the role of the mitochondrial ETC in immortalized mouse embryonic fibroblasts (iMEFs) in their acute response to proinflammatory lipopolysaccharides (LPS) and the prohypertrophic angiotensin II (Ang-II). LPS and Ang-II were administered over a 24-hour period to iMEFs cultured in media containing glucose or galactose promoting glycolysis and oxidative phosphorylation (OXPHOS), respectively. In addition, we used alternative oxidase (AOX), a molecular bypass of the cytochrome segment of the ETC and a rescue mechanism found in plants, yeasts, and many lower organisms, but not in insects or vertebrates. When expressed as a xenogene, AOX has proven indispensable in previous studies for investigating disease mechanisms in mammalian cells and animal models under various stress conditions in vivo[9,24–28].

We found that both LPS and Ang-II elicit an upregulation of proinflammatory genes, which was partially attenuated by AOX. As expected, cellular oxygen consumption rates (OCRs) were higher in galactose media, but despite a clear proinflammatory signaling response suggesting a shift in cellular phenotype, OCRs remained stable irrespective of treatments. We conclude that fibroblasts elicit a similar proinflammatory response to mechanistically distinct stressors, which is modulated by ETC activity. The magnitude of OCRs, however, does not permit conclusions regarding the extent of the inflammatory response.

Results

Immortalized mouse embryonic fibroblasts (iMEFs) cell culture model

To study the role of the ETC in the acute response of fibroblasts to stress stimuli, we decided to use a previously established and validated cell culture model, i.e., immortalized mouse embryonic fibroblasts (iMEFs) isolated from a mouse model globally expressing AOX (AOX^{Rosa26}) and WT littermates[29,30]. AOX expression was essential for the purpose of the study, as it can bypass the cytochrome segment of the ETC thereby restoring electron flux and decreasing the production of reactive oxygen species[26,31,32]. Importantly, AOX is biologically inert in mice even when constitutively expressed as its catalytic engagement is restricted to a disrupted ETC[29]. We first tested whether AOX expression had an effect on the overall cell growth or morphology of iMEFs. Irrespective of their genotype, WT and AOX-expressing iMEFs were indistinguishable by light microscopy and exhibited the typical spindle-shaped morphology (Fig. 1A). In cell culture media containing glucose as the main carbon source, both WT and AOX-expressing iMEFs proliferated at a similar rate, with an estimated doubling time of ~ 24 h, as determined in three independent experiments by cell counting using a standard hemocytometer. Notably, glucose is a fast-metabolizing glycolytic substrate allowing high growth rates at the expense of lactate production. Conversely, galactose can also serve as a carbon source, even though it is metabolized more slowly, because it promotes OXPHOS, a particularly efficient form of energy metabolism[33]. Indeed, we observed a modestly slower doubling time of ~ 1.5 days, which nevertheless was similar in both genotypes.

Next, we confirmed correct genotypes at the level of genomic DNA (Fig. 1B) and AOX protein expression in cell lysates (Fig. 1C; Supplementary Fig. 1). To test if AOX is correctly sorted to the mitochondrial compartment, we used immunofluorescence staining. A custom-made AOX antiserum[34] was used and confirmed a typical mitochondrial pattern in AOX-expressing iMEFs (Fig. 1D) while giving only a low non-specific background signal in WT iMEFs. To estimate ETC activity in cultured iMEFs and to test if AOX is catalytically engaged, we monitored oxygen consumptions rates (OCRs) in real time using Resipher (Lucid Scientific) (Fig. 1E, F). Based on the traces (Fig. 1E), however, it was not possible to draw conclusions about where within the cells the oxygen

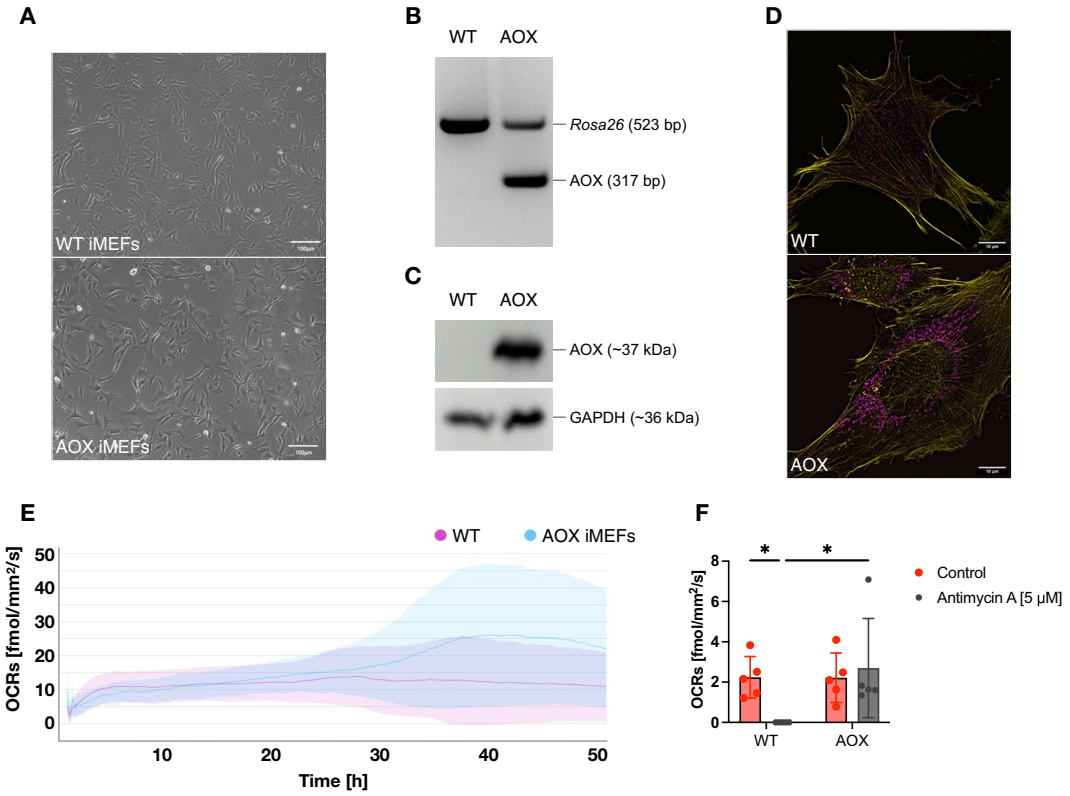


Fig. 1. Establishing and validating immortalized mouse embryonic fibroblasts (iMEFs) cultured in glucose media. (**A**) Representative light microscopy images of WT and AOX-expressing iMEFs as indicated. Scale bars in A denote 100 µm. (**B**) Validation of iMEFs genotypes. PCR fragments separated on agarose gel and stained by ethidium bromide. bp, base pairs. WT, partial *Rosa26 locus*; AOX, partial AOX cDNA. (**C**) Western blots demonstrating AOX expression with glyceraldehyde-3-phosphate dehydrogenase (GAPDH) serving as loading control (also see Supplementary Fig. 1). (**D**) Representative immunofluorescence images of WT and AOX-expressing iMEFs as indicated. AOX (visualized using false-color magenta) was detected using a custom-made AOX antiserum giving rise to low non-specific background in WT and a typical mitochondrial pattern in AOX-expressing iMEFs. The actin cytoskeleton was stained with Phalloidin-Alexa Fluor 488 (shown in yellow). Images were taken with multi-color structured illumination microscopy. Scale bars denote 10 µm. (**E**) Original traces showing oxygen consumption of WT and AOX-expressing iMEFs as in presence of complex III inhibitor antimycin A (5 µM). Antimycin A was added 24 h after cell seeding. Pink represents OCRs of WT-iMEF, and blue represents OCRs AOX-iMEF. The lines indicate mean values of $n = 6$ continuously measured technical replicates. The "shadows" indicate error bars, i.e., SEM. (**F**) Quantification of OCRs in WT and AOX-expressing iMEFs over a 24-hour period in the presence and absence of antimycin A, as indicated, validating inhibitor resistance specifically in AOX-expressing iMEFs. Data are shown as mean ± SD of $n = 5$ independent experiments. *$p \leq 0.05$ assessed by two-way ANOVA multiple comparisons and uncorrected Fisher's LSD *post hoc* test.

is consumed. We therefore added an inhibitor of complex III of the ETC, antimycin A. Under these conditions, oxygen consumption in WT iMEFs essentially ceased, while AOX-expressing cells continued respiring (Fig. 1E, F). Interestingly, despite treatment with antimycin A, respiratory activity in AOX-expressing iMEFs is virtually the same as in uninhibited WT iMEFs, supporting previous findings that AOX respiration does not function additively but only engages catalytically when electron flux through the ETC is disrupted[26]. In summary, the data show good AOX expression in iMEFs, which are otherwise similar to WT iMEFs in terms of phenotype and proliferation behavior. AOX correctly sorts to the mitochondrial compartment and is catalytically active. This makes the combination of WT and AOX-expressing iMEFs a suitable model for testing the role of the ETC in response to inflammatory stress stimuli.

Proinflammatory gene expression is modified by ETC activity

By using these cell culture models that can be converted to different metabolic states (glycolysis vs. OXPHOS) in the presence or absence of a genetic rescue mechanism (AOX), we set out to test their acute response to proinflammatory stressors. We treated iMEFs for 24 h with two factors known to provoke proinflammatory stress in fibroblasts using two different concentrations each, i.e., 10–20 µg LPS/mL culture medium, and 200 nM or 400 nM Ang-II. Since LPS above a critical threshold can induce cell death, we conducted titration tests before beginning our actual experiments. Cell death was not observed until concentrations of 30 µg LPS/mL

culture medium were reached. To induce measurable changes in cytokine expression and to simulate a strong inflammatory response rather than subtle endotoxin signaling, we decided to use 10 µg and 20 µg LPS/mL culture medium.

We selected six transcripts held responsible to monitor proinflammatory response at different levels, from essential receptors to effectors, i.e., toll-like receptor 4 (*Tlr4*), interleukin 6 (*Il6*), transforming growth factor, beta 1 (*Tgfb1*), NLR family, pyrin domain containing 3 (*Nlrp3*), caspase 1 (*Casp1*) and interleukin 1 beta (*Il1b*). Transcript levels were assessed by RT-qPCR and normalized to the housekeeping gene beta actin (*Actb*). We found that both LPS (Fig. 2A-R) and Ang-II (Fig. 3A-R) induced proinflammatory genes mostly in a dose-dependent manner yet revealed notable differences with regard to carbon source and ETC activity.

In general, LPS induced a robust concentration-dependent induction of proinflammatory genes in an AOX-sensitive manner, with one exception (*Nlrp3*) (Fig. 2J-L). Interestingly, substrate use exerted its influence in different ways. In some cases (e.g., *Tlr4*) (Fig. 2A-C), we observed similar effects from 10 µg/mL LPS in galactose media as from 20 µg/mL LPS in glucose media suggesting that oxidative metabolism sensitizes iMEFs to the stressor. In other cases (e.g., *Casp1*) (Fig. 2M-O), gene expression seemed to be primarily dependent on LPS concentration. Especially at higher concentrations of 400 nM, Ang-II also induced most of the pro-inflammatory genes (Fig. 3A-R). However, overall gene expression was less sensitive to AOX. The data thus show that seemingly different stress stimuli elicit a similar proinflammatory response in gene expression. The observed sensitivity to AOX, particularly in the case of LPS, supports the notion that ETC activity is relevant for cellular response upon stress.

The increase in gene expression is partially reflected in cytokine secretion

To assess whether the aforementioned induction of gene expression corresponds to cytokine secretion, we measured selected proteins in cell culture media. Immunolabeling was done using a cytokine bead array and quantification was achieved using a flow cytometer. In addition to IL-6 and IL-1β, we also measured C-C motif chemokine ligand 2 (CCL2 *aka* monocyte chemoattractant protein-1, MCP1). We found that LPS (Fig. 4A-I) and Ang-II (Fig. 5A-I) treatments resulted in only subtle differences. Notably, LPS treatment resulted in an increase in secreted IL-6, which was attenuated by AOX (Fig. 4B, C). Conversely, CCL2 even decreased under LPS treatment but only in WT iMEFs cultured in galactose media (Fig. 4I). Although the differences in protein expression are relatively small, likely due to the design of the experiments, the data show that the proinflammatory response is not confined to the transcriptional level.

Oxygen consumption rates (OCRs) respond to metabolic states but not to AOX and/or proinflammatory stimuli

Previously, it was shown that functioning of the ETC is essential for oxygen sensing in pulmonary arterial smooth muscle cells[32], response to endotoxemia in macrophages[35] and NLRP3 inflammasome activation in $CD8^+$ T cells[36]. We thus wanted to explore whether the observed shifts toward proinflammatory gene expression under LPS or Ang-II treatment, with varying dependencies on substrate utilization and molecular ETC bypass, were somehow reflected in altered cellular OCRs. Again, we used Resipher (Lucid Scientific) and found slight differences in OCRs depending on the substrate, i.e., iMEFs appeared to have higher OCRs in galactose compared to glucose media (Fig. 6). Somewhat surprisingly, OCRs appeared to be completely unaffected by treatment with LPS and Ang-II in the presence or absence of AOX. This suggests that the overall flux of electrons through the ETC is similar regardless of the treatment.

Mitochondrial morphology in WT but not in AOX iMEFs responds to proinflammatory stress

Knowing that bioenergetic function is intimately tied to mitochondrial shape[37], we visualized mitochondria under treatment with LPS and Ang-II using structured illumination super-resolution microscopy (SIM)[38]. Again, iMEFs were cultured under standard conditions using glucose as main carbon source and treated with 10 µg/mL LPS and 200 nM Ang-II (Fig. 7). Mitochondrial morphology was visualized by SIM imaging of MitoTracker Deep Red FM together with actin cytoskeleton (palloidin-AlexaFluor488). Of note, WT iMEFs, mitochondria overall exhibited a more filamentous and interconnected phenotype, whilst in AOX-expressing iMEFs they showed a more condensed, spherical structure (**insets in** Fig. 7). Interestingly, both LPS and Ang-II induced a more dispersed distribution in WT iMEFs, more or less phenocopying the morphology in AOX iMEFs, while in the latter, mitochondrial morphology appeared relatively unchanged.

Discussion

In recent years, organ-resident fibroblasts emerged as essential signaling hubs in health and disease. While managing tissue integrity and organ function under physiological conditions, fibroblasts start proliferation, switch phenotype and initiate proinflammatory signal transduction upon stress[1–4]. Factors initiating such switch are remarkably diverse and apparently dependent on organ and tissue composition. In the heart, for example, fibroblasts react to increased wall tension due to pressure overload, but also to inflammation in sepsis, which in both cases can culminate in contractile dysfunction[5,8,13,14]. In this report we demonstrate that cultured iMEFs (Figs. 1 and 7) respond to seemingly unrelated stress factors, LPS (endotoxins from the outer membrane of gram-negative bacteria) and Ang-II (a prohypertrophic octapeptide and key vasoconstrictor in the renin-angiotensin system), with the activation of proinflammatory genes in a similar manner (Figs. 2 and 3).

LPS-induced endotoxemia is a well-established experimental model to elucidate sepsis-related inflammatory response mechanisms in model organisms and at the cellular level. Indeed, LPS exposure resulted in a robust proinflammatory response in iMEFs. Key sensor for LPS is the toll-like receptor 4 (TLR4) known to activate

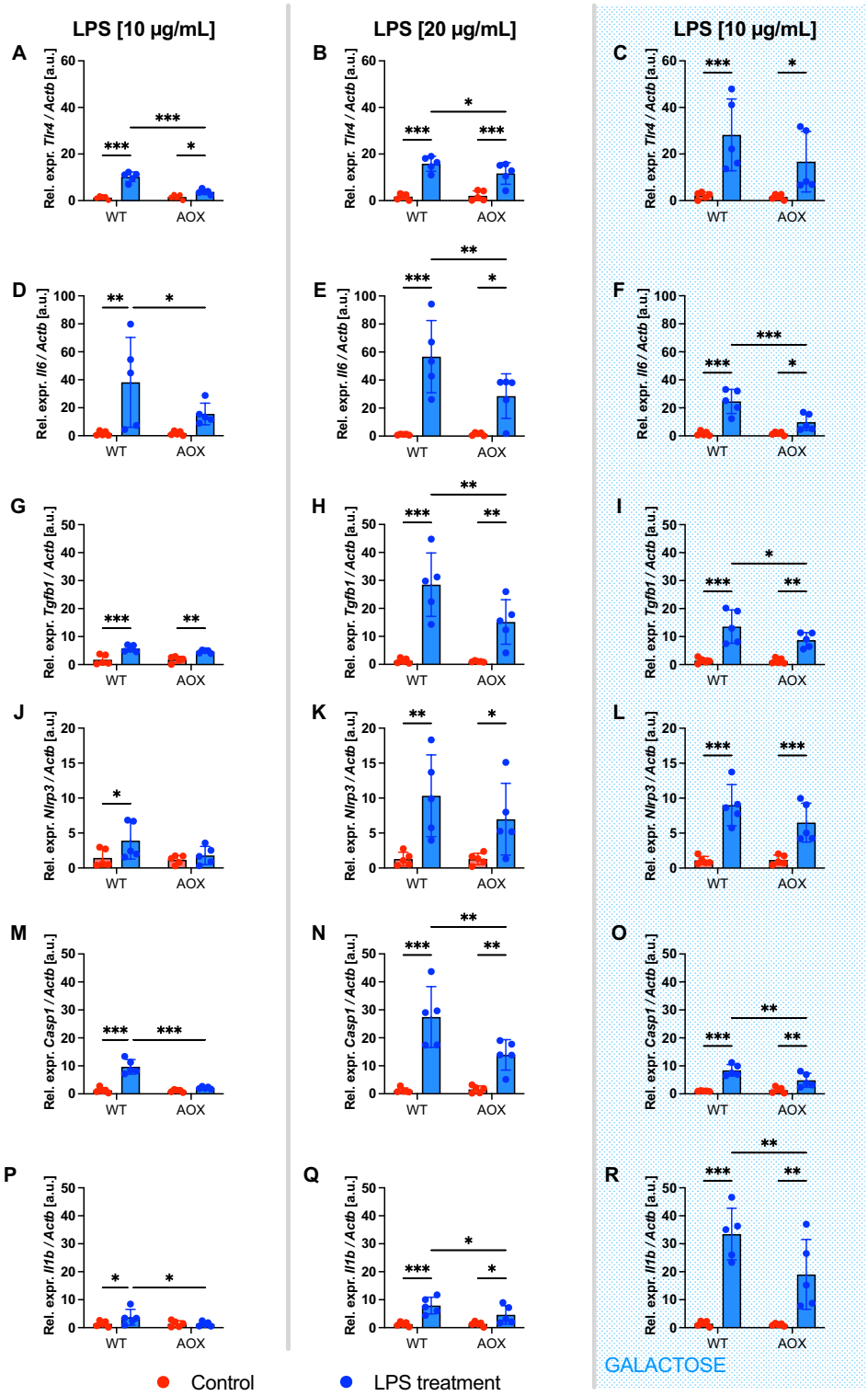


Fig. 2. Relative mRNA expression level in LPS-treated iMEFs. Transcript levels from RT-qPCR reactions were calculated using the $2^{-}\Delta\Delta Ct$ method. Beta actin (*Actb*) served as housekeeping gene. WT and AOX-expressing iMEFs were cultured in glucose- (**A**, **B**, **D**, **E**, **G**, **H**, **J**, **K**, **M**, **N**, **P**, **Q**) and galactose- (**C**, **F**, **I**, **L**, **O**, **R**) containing media and treated with the endotoxin lipopolysaccharide (LPS) 10–20 µg/mL as indicated. (**A-C**) *Tlr4* - toll-like receptor 4. (**D-F**) *Il6* - interleukin 6. (**G-I**) *Tgfb1* - transforming growth factor, beta 1. (**J-L**) *Nlrp3* - NLR family, pyrin domain containing 3. (**M-O**) *Casp1* - caspase 1. (**P-R**) *Il1b* - interleukin 1 beta. Data are shown as mean ± SD in arbitrary units [a.u.] of $n = 5$ independent experiments. $^{*}p \leq 0.05$, $^{**}p \leq 0.01$, $^{***}p \leq 0.001$ assessed by two-way ANOVA multiple comparisons and uncorrected Fisher's LSD *post hoc* test.

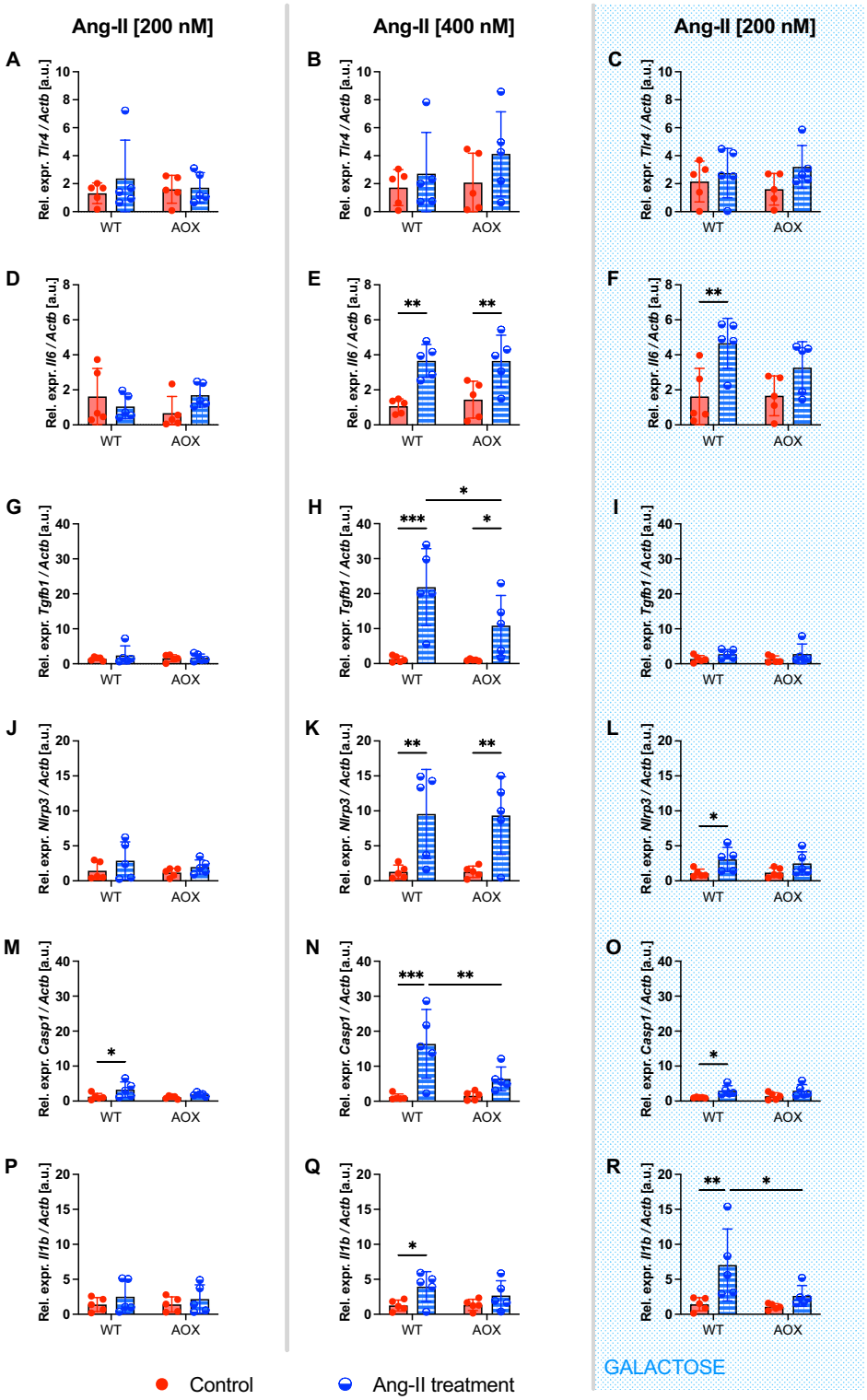


Fig. 3. Relative mRNA expression level in Ang-II-treated iMEFs. Transcript levels from RT-qPCR reactions were calculated using the $2^{-}\Delta\Delta Ct$ method. Beta actin (*Actb*) served as housekeeping gene. WT and AOX-expressing iMEFs were cultured in glucose- (**A**, **B**, **D**, **E**, **G**, **H**, **J**, **K**, **M**, **N**, **P**, **Q**) and galactose- (**C**, **F**, **I**, **L**, **O**, **R**) containing media and treated with the prohypertrophic factor Angiotensin (Ang-II) 200 or 400 nM as indicated. (**A-C**) *Tlr4* - toll-like receptor 4. (**D-F**) *Il6* - interleukin 6. (**G-I**) *Tgfb1* - transforming growth factor, beta 1. (**J-L**) *Nlrp3* - NLR family, pyrin domain containing 3. (**M-O**) *Casp1* - caspase 1. (**P-R**) *Il1b* - interleukin 1 beta. Data are shown as mean ± SD in arbitrary units [a.u.] of $n = 5$ independent experiments. $^{*}p \leq 0.05$, $^{**}p \leq 0.01$, $^{***}p \leq 0.001$ assessed by two-way ANOVA multiple comparisons and uncorrected Fisher's LSD *post hoc* test.

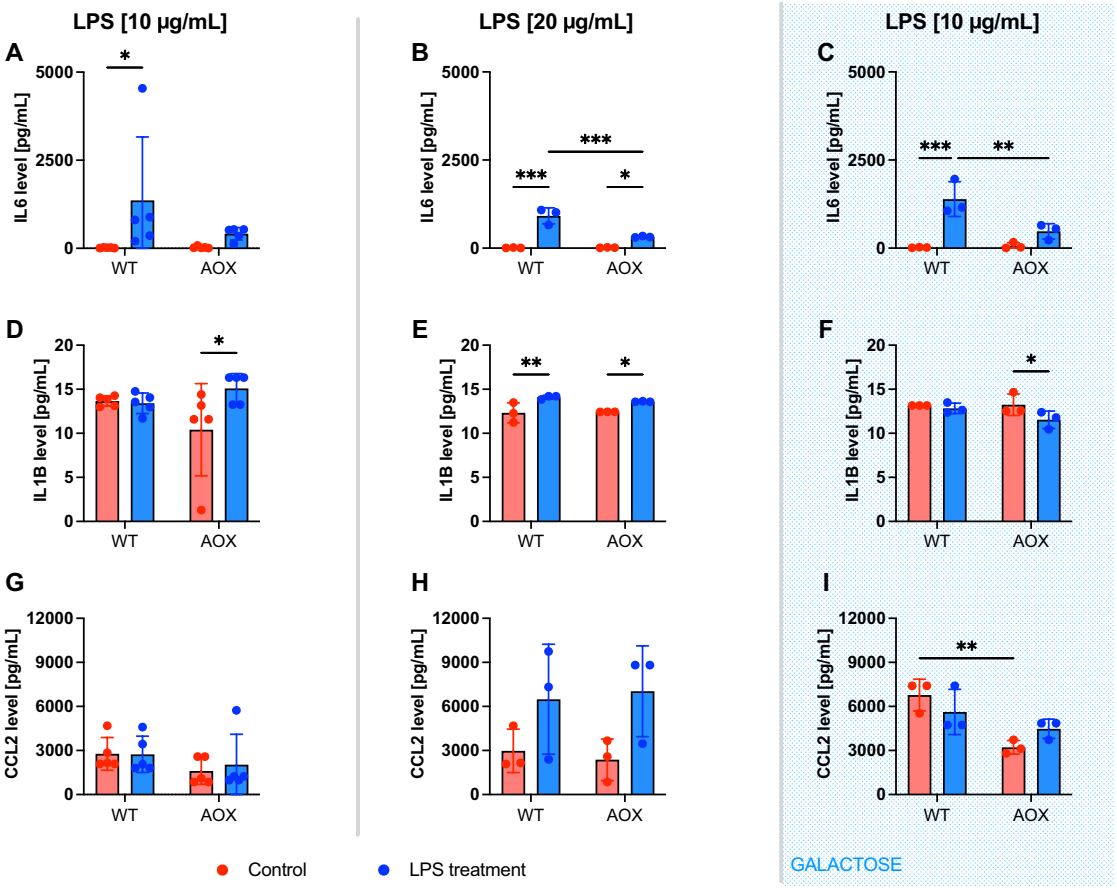


Fig. 4. Absolute protein concentrations measured by Cytometric Bead Array (CBA) in cell culture media from LPS-treated iMEFs. WT and AOX-expressing iMEFs were cultured in glucose- and galactose-containing media and treated with LPS 10–20 µg/mL as indicated. (**A-C**) IL-6 - interleukin 6. (**D-F**) IL-1β - interleukin 1 beta. (**G-I**) CCL2 - C-C motif chemokine ligand 2 (*aka* MCP1, monocyte chemoattractant protein-1). Data are shown as mean ± SD in pg/mL of $n = 5$ (LPS 10 µg/mL in glucose media) or $n = 3$ (LPS 20 µg/mL in glucose media and LPS 10 µg/mL in galactose media) independent experiments. $^{*}p \leq 0.05$, $^{**}p \leq 0.01$, $^{***}p \leq 0.001$ assessed by two-way ANOVA multiple comparisons and uncorrected Fisher's LSD *post hoc* test.

MyD88 and Toll/IL-1R-domain-containing adaptor-inducing IFN-β (TRIF). Stimulation of these pathways leads to downstream activation of signaling cascades including NF-κB and MAPKs, which then induce the transcription of inflammatory and profibrotic genes, including IL-6, IL-1β and TGFβ1 (Fig. 2)[39,40]. LPS is also known to activate inflammasome-associated factors in fibroblasts, supported by an increased expression of NLRP3 and CASP1[13]. Our data support the concept of LPS-specific cellular response in fibroblasts.

Similarly, albeit to a lesser degree, Ang-II induced a proinflammatory gene expression in iMEFs, characterized by increased *Il6* and *Tgfb1* expression and modest activation of *Nlrp3*, *Casp1* and *Il1b* (Fig. 3). In contrast to LPS, Ang-II did not induce *Tlr4* expression possibly hinting mechanistic differences between pathogen-associated and non-infectious inflammatory conditions. In line with this notion, Ang-II is thought to promote fibroblast inflammation through angiotensin 1 (AT_1) receptor-dependent oxidative stress rather than classical TLR-mediated signaling. Indeed, previous studies using cardiac fibroblasts have demonstrated that Ang-II triggers NLRP3 inflammasome assembly and CASP1 activation through AT_1 receptor signaling in a calcium-dependent manner, eventually resulting in IL-1β secretion[41]. Importantly, cardiac fibroblasts have also been identified as a site of inflammasome activation in ischemia-reperfusion injury, supporting the concept that fibroblasts contribute actively to sterile inflammation[42].

In cardiomyocytes, activation of the NLRP3 inflammasome in response to non-ischemic stress and NF-κB-dependent priming was accompanied by an increase in *Nlrp3* gene expression, which eventually enables the processing of downstream factors such as IL-1β and IL-18[43,44]. The rather modest induction of *Nlrp3*, *Casp1*, and *Il1b* observed in our study thus aligns with the literature and suggests that Ang-II may act as a relatively weak or context-dependent inflammasome activator in fibroblasts. Full inflammasome activation and substantial *Il1b* expression and IL-1β secretion may require longer incubation time, higher concentrations or additional co-stimulatory signals.

The observed induction of *Il6* and *Tgfb1* transcripts is also consistent with established Ang-II-AT_1 receptor-driven profibrotic signaling pathways. Cardiac and renal fibroblasts have been shown to respond to Ang-II by upregulation of *Il6*, *Tgfb1* as well as fibrotic markers such as collagen I and α-smooth muscle actin (*Acta2*).

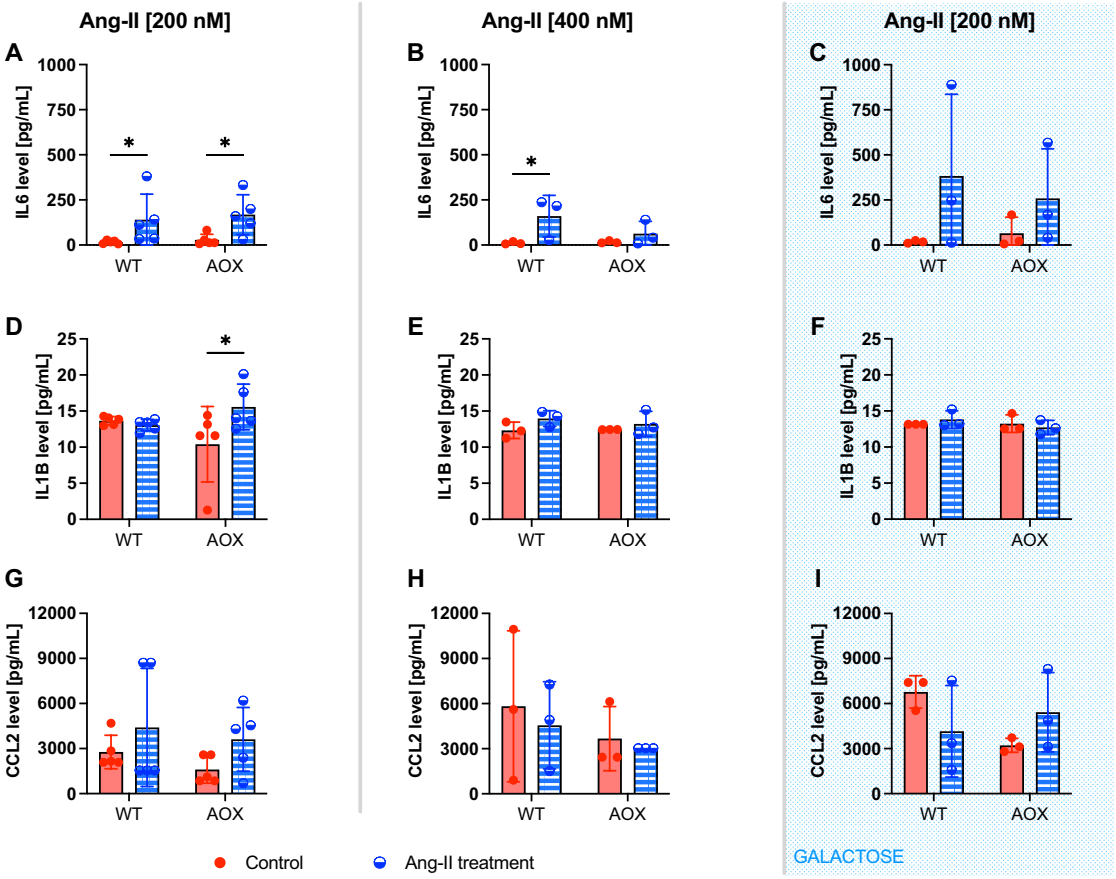


Fig. 5. Absolute protein concentrations measured by Cytometric Bead Array (CBA) in cell culture media from Ang-II-treated iMEFs. WT and AOX-expressing iMEFs were cultured in glucose- and galactose-containing media and treated with Ang-II 200 or 400 nM as indicated. (**A-C**) IL-6 - interleukin 6. (**D-F**) IL-1β - interleukin 1 beta. (**G-I**) CCL2 - C-C motif chemokine ligand 2 (*aka* MCP1, monocyte chemoattractant protein-1). Data are shown as mean ± SD in pg/mL of $n = 5$ (Ang-II 200 nM in glucose media) or $n = 3$ (Ang-II 400 nM in glucose media and Ang-II 200 nM in galactose media) independent experiments. $^{*}p \leq 0.05$ assessed by two-way ANOVA multiple comparisons and uncorrected Fisher's LSD *post hoc* test.

Furthermore, Ang-II-AT_1 receptors signaling promotes fibroblast-to-myofibroblast differentiation, a process central to fibrosis and adverse cardiac remodeling[45–47]. Fibroblast activation and proliferation is regulated by an integration of neurohumoral, mechanical, and inflammatory signals, with TGFβ1 acting as a key driver[48]. Overall, this directly links Ang-II signaling to inflammation and fibrosis and may provide insights into why Ang-II and LPS activate proinflammatory responses in a similar but not identical manner and underscores the validity of our findings.

One of the many unresolved questions in proinflammatory stress response is the role of the mitochondrial ETC. We and others have previously shown that the ETC has sensing and signaling functions beyond ATP production[27,32,35,49–52]. To test how the ETC might be involved, different approaches were taken: (**i**) we used cell culture media with different primary carbon sources, i.e., glucose and galactose, forcing cells into a more glycolytic and oxidative metabolic state, respectively[33]; (**ii**) concomitant to WT iMEFs we used iMEFs xenotopically expressing AOX, a molecular bypass if electron flux through the ETC is disrupted. Indeed, our data show differential responses to LPS and Ang-II in activation of proinflammatory genes depending on oxidative metabolism and restoration of ETC function (Figs. 2 and 3). We also examined selected cytokines at the protein level in cell culture medium and found that their secretion partially followed the transcriptional activation (Figs. 4 and 5). The relatively weak response at the protein level is probably not surprising, since we were interested in acute cellular responses following a relatively short exposure time of only 24 h to the stressor. Interestingly enough, IL-6 secretion is significantly increased upon LPS and Ang-II treatment and in the case of LPS even in an AOX-sensitive manner (Fig. 4B, C).

The combination of different approaches, all of which appear to target the ETC function, i.e., different carbon sources and ETC restoration, allowed insight into different functions of the ETC. For instance, while galactose media promote oxidative metabolism, cells in glucose media are less dependent on it. Restoration of electron flux through the ETC may thus have synergistic, complementary or antagonistic consequences. Indeed, some highly proliferative cells such as cancer cells rely on glycolysis despite the presence of oxygen, a phenomenon also known as oxidative glycolysis or the Warburg effect[53]. Proliferating cells may rely on it to meet the prevailing

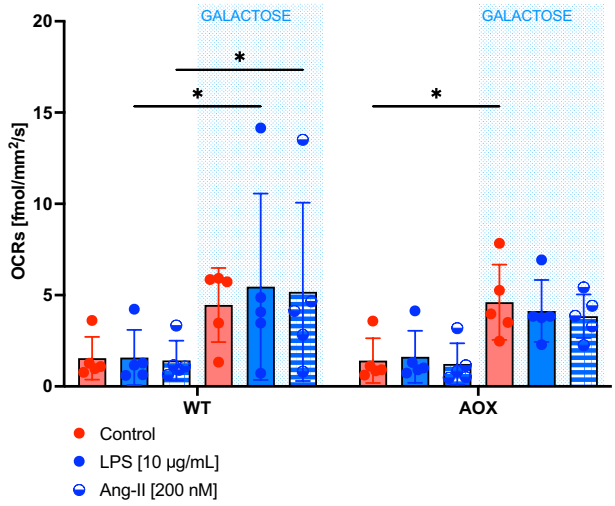


Fig. 6. Gradient O_2 flux measurement and comparison of OCRs depending on main substrate and inhibitor treatment. WT and AOX-expressing iMEFs were cultured in glucose- and galactose-containing media and treated with LPS 10 µg/mL and Ang-II 200 nM as indicated. Oxygen consumptions rates (OCRs) of cultured iMEFs were calculated from Resipher raw data. Data are shown as mean ± SD in fmol/mm^2/s of $n = 5$ independent experiments. $^*p \leq 0.05$ assessed by two-way ANOVA multiple comparisons and uncorrected Fisher's LSD *post hoc* test.

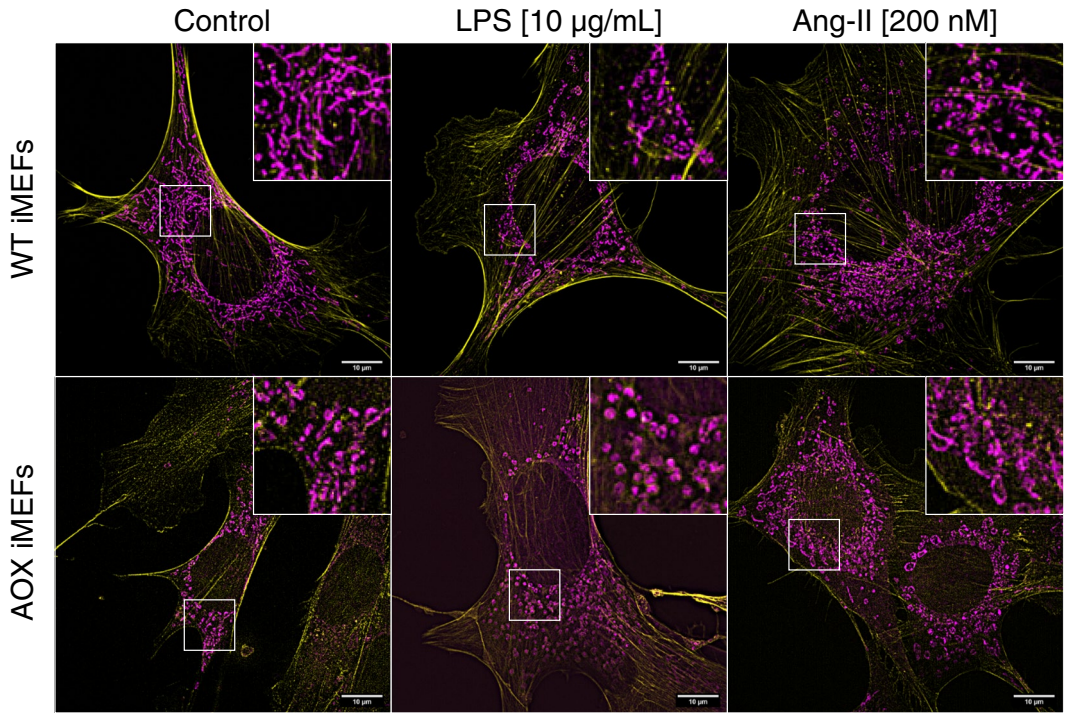


Fig. 7. Representative super-resolution structured illumination microscopy of MitoTracker staining in WT and AOX-expressing iMEFs. WT and AOX-expressing iMEFs were cultured in standard glucose-containing media and treated for 24 h with LPS 10 µg/mL and Ang-II 200 nM as indicated. Mitochondria were stained with MitoTracker Deep Red (magenta) and the actin cytoskeleton was stained with Phalloidin-Alexa Fluor 488 (yellow) and imaged with multi-color structured illumination microscopy. Of note, mitochondria in WT-iMEFs appear more filamentous and interconnected as a mitochondrial network, whereas mitochondria in AOX-expressing iMEFs are more condensed (insets). In WT, treatment shifts the mitochondrial phenotype toward separation. In AOX, no significant change in mitochondrial morphology was observed. Scale bars denote 10 µm.

cellular need, i.e., replenishing NAD^+ instead of ATP production[54]. Uncoupling of electron flux through the ETC may thus be advantageous and change the signaling behavior as observed in the stress response of treated iMEFs. In fact, as expected, OCRs changed depending on the main carbon source, but surprisingly did not respond to LPS and Ang-II or to xenotopic expression of AOX (Fig. 6). Nevertheless, the presence of AOX altered gene expression patterns, suggesting an essential role for the ETC. However, based on our findings, the diagnostic value of OCRs alone is debatable, as oxygen consumption alone appears to be a poor marker of mitochondrial (dys)function. Of course, it would be interesting to know what happened to oxygen, if the ETC was indeed uncoupled, produced more reactive oxygen species, or if alternative oxygen-consuming processes were activated. It would be equally important to know by which mechanism AOX influenced gene expression, e.g., excessive loads of reactive oxygen species or a redox imbalance. All of these questions merit further research.

Mitochondria dynamically change their morphology, and in fact their shape is closely linked to bioenergetics[37]. Upon treatment with LPS and Ang-II, we observed differences in mitochondrial nanoscale morphology in WT iMEFs but not in AOX-expressing iMEFs. In WT iMEFs, the mitochondrial shape shifted from a filamentous and interconnected towards a condensed and fragmented phenotype. A shift from elongated to more scattered mitochondria has previously been observed in a disease model[52]. Whether the observed AOX-mediated effect is based on the same mechanism remains to be tested. For instance, a systematic approach based on a quantitative morphological analysis of the nanoscale mitochondrial network[55] may reveal subtle phenotypical changes in large cellular populations.

Taken together, in this report we show that inflammatory and hypertrophic stimuli can induce a similar proinflammatory phenotype shift in fibroblasts. The use of different carbon sources, glucose vs. galactose, and the expression of a molecular bypass of the ETC, AOX, indicate an essential role of the ETC on cellular signaling behavior in proinflammatory stress response of fibroblasts. Confusingly, a seemingly essential role of electron flux through the ETC is not reflected in changes in OCRs. The molecular mechanisms underlying these observations remain to be elucidated.

Methods

Culturing immortalized mouse embryonic fibroblasts (iMEFs)

Embryonic fibroblasts were previously isolated from a genetically trackable mouse model expressing *Ciona intestinalis* AOX[29] and immortalized (iMEFs) as described elsewhere[30,56]. iMEFs were cultured in media with different primary carbon sources, i.e., glucose (essentially fast-metabolizing, yielding high growth but promoting lactate production) or galactose (slower-metabolizing, enhancing OXPHOS)[33]. (**i**) Glucose media composition: Dulbecco's Modified Eagle Medium (DMEM, PAN Biotech, P04-01500) supplemented with 100 µg/mL streptomycin and 100 U/mL penicillin (ThermoFisher Scientific, 15140122), and 20% fetal bovine serum (FBS, Sigma-Aldrich, F7524). (**ii**) Galactose media composition: Roswell Park Memorial Institute (RPMI) 1640 Medium (Gibco, 11879020) supplemented with 100 µg/mL streptomycin and 100 U/mL penicillin, 20% FBS, 1 mM sodium pyruvate (ThermoFisher Scientific) and 10 mM D-(+)-galactose (Carl Roth, 4987.1). Cells were cultured at 37 °C, 5% carbon dioxide in a humidified atmosphere. Growth media were changed every 48 h and cells were cultured until reaching a maximal confluency of 80%. iMEFs were treated with lipopolysaccharides (LPS) from *Escherichia coli* EH100 (Sigma-Aldrich, L9641) at concentrations of 10–20 µg LPS/mL culture medium, human Angiotensin II (Sigma-Aldrich, A9525) at concentrations of 200 or 400 nM, or antimycin A (Sigma-Aldrich, A8674), as indicated in the text, figures and legends.

Genotyping of iMEFs

Genomic DNA was extracted from iMEFs using the DNeasy Blood & Tissue Kit (QIAGEN, 69506). Genotyping PCR was carried out using AccuStart II PCR SuperMix (Quantabio, 733–2242) essentially as previously described[29]. Primers used for WT *Rosa26* locus (5'-3'): forward GACCTCCATCGCGCACTCCG, reverse CTC CGAGGCGGATCACAAGC (fragment length 523 bp). Primers used for AOX coding sequence (5'-3'): forward GCGATGCAAGATGGAGGGTA, reverse TGAATCCAACCGTGGTCTCG (fragment length 317 bp).

Protein extraction and immunoblotting

iMEFs were harvested in lysis buffer [0.4 mM Tris-HCl (pH 7.5) (Sigma-Aldrich, T3253), 0.4 mM NaCl (Carl Roth, 9265.1), 2.5 mM NaF (Sigma-Aldrich, S7920), 6 mM $Na_4P_2O_7$ (Sigma-Aldrich, S6422), 2 mM Na_3VO_4 (Sigma-Aldrich, S6508), 1% Triton X-100 (Sigma-Aldrich, T9284), 0.44 mM PMSF (Carl Roth, 6367.1), 1 tablet/10 mL cOmplete Protease Inhibitor Cocktail Tablets (Roche, 11697498001). After incubating on ice for 30 min, the lysate was centrifuged at 12,500 x g and 4 °C for 10 min. The supernatant containing the concentrated protein was stored at -80 °C until use. Total protein concentration was quantified using the Protein Assay Dye Reagent (Bio-Rad, 5000006). Proteins were separated on 12% SDS polyacrylamide gels and transferred to polyvinylidene fluoride (PVDF) membranes (Carl Roth, T831.1) using the wet blot system (Bio-Rad, Mini-PROTEAN Tetra Cell and Mini Trans-Blot Module, 1658029). Membranes were probed using anti-AOX customized rabbit antiserum (21st Century Biochemicals, 1:10,000)[34] and anti-GAPDH antibody (Abcam, ab37168, 1:1,000). Secondary antibody was rabbit IgG HRP Linked Whole Ab (Merck, GENA934, 1:30,000).

Gene expression (RT-qPCR)

Total RNA was isolated using the RNeasy Mini Kit (QIAGEN, 74104) following the manufacturer's instructions and mRNA was stored at -80°C until use. RNA concentration and quality was assessed by light absorbance measured at 260 nm and 280 nm using a NanoDrop ND-1000 spectrophotometer (Thermo Scientific). Isolated RNA was reverse-transcribed to cDNA using the SensiFAST SYBR No-ROX One-Step Kit (meridian BIOSCIENCE, BIO-72005) according to the manufacturer's instructions. cDNA amplification and quantification was done using a Rotor-Gene Q real-time PCR cycler (QIAGEN, 9001862). The following primers were used: *Mus musculus* toll-

like receptor 4 (*Tlr4*) (NM_021297.3) cDNA (5'-3'): forward CTCAGCAAAGTCCCTGATGACA, reverse TCA ATTGTTTCAATTTCACACCTGG (fragment length 149 bp); *Mus musculus* interleukin 6 (*Il6*) (NM_031168.2) cDNA (5'-3'): forward GTGGAAATGAGAAAAGAGTTGTGC, reverse TAGGAGAGCATTGGAAATTGGG G (fragment length 336 bp). *Mus musculus* transforming growth factor, beta 1 (*Tgfb1*) (NM_011577.2) cDNA (5'-3'): forward TGATACGCCTGAGTGGCTGTCT, reverse CACAAGAGCAGTGAGCGCTGAA (fragment length 107 bp). *Mus musculus* NLR family, pyrin domain containing 3 (*Nlrp3*) (NM_145827.4) cDNA (5'-3'): forward TGGGTTCTGGTCAGACACGAG, reverse GGGGCTTAGGTCCACACAGAAA (fragment length 176 bp). *Mus musculus* caspase 1 (*Casp1*) (NM_009807.2) cDNA (5'-3'): forward GGCACATTTCCAGGACTG ACTG, reverse GCAAGACGTGTACGAGTGGTTG (fragment length 125 bp). *Mus musculus* interleukin 1 beta (*Il1b*) (NM_008361.4) cDNA (5'-3'): forward TGCCACCTTTTGACAGTGATG, reverse AAGGTCCACGGGA AAGACAC (fragment length 220 bp). *Mus musculus* actin, beta (*Actb*) (NM_007393.5) cDNA (5'-3'): forward C CCAGATCATGTTTGAGACCT, reverse CCATCACAATGCCTGTGGTA (fragment length 102 bp).

Immunolabeling and quantification of secreted proteins using Cytometric Bead Array (CBA)

Cytokines and chemokines were quantified using the BD Cytometric Bead Array (CBA) Mouse Inflammation Kit (BD Biosciences, 552364) and the BD Cytometric Bead Array (CBA) Mouse/Rat Soluble Protein Master Buffer Kit (BD Biosciences, 558266) according to the manufacturer's instructions. Briefly, cell culture media were collected 24 h after treatment with LPS or Ang-II. 50 µL of each sample and freshly reconstituted serially diluted standards were incubated for 1 h at room temperature with 50 µL of the mixed Mouse Inflammation Capture Bead suspension containing anti-cytokine antibody-coated beads. Afterwards, 50 µL of the phycoerythrin-conjugated detection antibody reagent was added to each sample and incubated for an additional 1 h. Unbound antibodies were washed off using the washing buffer and centrifuged at 200 x g for 5 min. The pellet was resuspended in 300 µL washing buffer. Fluorescence was measured and analyzed using the BD FACSCanto flow cytometer and software (CytoFLEX, Beckman). A total number of 4,000 events per sample were captured.

Assessment of oxygen consumption rates (OCRs)

Oxygen consumption rates (OCRs) were measured using the Resipher (Lucid Scientific), which enables real-time monitoring of OCRs in living cells for over 24 h. The system consists of a lid equipped with an array of 32 ultra-sensitive sensors that detect dissolved oxygen. For real-time monitoring, data are streamed to "Lucid Lab" for cloud-based analysis. During data acquisition, the sensors perform dynamic micro-movements in the Z axis, allowing OCRs to be calculated based on the oxygen gradient within the culture media generated by metabolically active cells. Measurements rely on an oxygen-sensitive material at each sensor tip, which detects dissolved oxygen quenching of a wavelength in the range of 435–485 nm. The signal quenching by dissolved oxygen in native cell culture media is then converted into actual oxygen concentrations. An initial equilibration period of 1 h is required to establish a stable gradient within the media. To minimize the influence of external variables, the Resipher also monitors environmental factors such as incubator temperature, relative humidity, and atmospheric pressure.

Immunocytochemistry and super-resolution imaging

An AOX customized rabbit antiserum (21st Century Biochemicals) was used essentially as previously described[34]. Mitochondria were stained using MitoTracker Deep Red FM (Invitrogen, M22426) at a final concentration of 500 nM in cell culture media for 20 min at 37.5 °C. Following incubation, cells were fixed with 3.2% formaldehyde in phosphate-buffered saline (PBS) (pH 7.4) for 20 min at room temperature. The actin cytoskeleton was stained with Phalloidin labeling probe Alexa Fluor 488 (Invitrogen, A12379) (1:200 dilution) for 30 min. Image acquisition was done using a ZEISS Elyra 7 widefield fluorescence microscope (Carl Zeiss Microscopy) equipped with lattice structured illumination microscopy (lattice-SIM). Images were acquired using a 63x objective (NA 1.4) with a 1.6x Optovar and the following acquisition parameters: exposure time 50 ms; laser intensities 10% (405 nm), 5% (488 nm), and 0.25% (647 nm). ZEISS ZEN Black software was used for image reconstruction. Images were adjusted for contrast and visibility using Fiji (ImageJ).

Statistical analyses

Statistical analyses were done using the GraphPad Prism (GraphPad Software). Two-way ANOVA multiple comparisons and uncorrected Fisher's LSD *post hoc* test were used for comparisons of at least $n = 3$ independent experiments and $p \leq 0.05$ were considered statistically significant.

Data availability

All data generated or analyzed during this study are included in this article.

Received: 20 March 2026; Accepted: 3 July 2026
Published online: 05 August 2026

References

1. Plikus, M. V. et al. Fibroblasts: Origins, definitions, and functions in health and disease. *Cell* **184**, 3852–3872 (2021).
2. Miki, H. & Manresa, M. C. Novel fibroblast phenotypes in homeostasis and chronic inflammation: From functions to potential regulators. *J. Physiol.* **601**, 2273–2291 (2023).
3. Younesi, F. S., Miller, A. E., Barker, T. H., Rossi, F. M. V. & Hinz, B. Fibroblast and myofibroblast activation in normal tissue repair and fibrosis. *Nat. Rev. Mol. Cell. Biol.* **25**, 617–638 (2024).
4. Zou, A. E., Kongthong, S., Mueller, A. A. & Brenner, M. B. Fibroblasts in immune responses, inflammatory diseases and therapeutic implications. *Nat. Rev. Rheumatol.* **21**, 336–354 (2025).

5. Díez, J., González, A. & Kovacic, J. C. Myocardial Interstitial Fibrosis in Nonischemic Heart Disease, Part 3/4 JACC Focus Seminar. *J. Am. Coll. Cardiol.* **75**, 2204–2218 (2020).
6. Frangogiannis, N. G. Cardiac fibrosis. *Cardiovasc. Res.* **117**, 1450–1488 (2020).
7. Song, S. et al. Cardiac fibroblast Foxm1 deficiency prevents pressure overload-induced cardiac remodeling via the Usp10/MKK6-p38γ MAPK axis. *Cell. Death Differ.* 1–14. https://doi.org/10.1038/s41418-025-01609-1 (2025).
8. Chen, H. et al. Decoding mechanosensitive genes in cardiac fibroblasts via 3D hydrogel models of fibrosis. *Sci. Rep.* **15**, 30484 (2025).
9. Dhandapani, P. K. et al. Hyperoxia but not AOX expression mitigates pathological cardiac remodeling in a mouse model of inflammatory cardiomyopathy. *Sci. Rep.* **9**, 12741 (2019).
10. Abe, H. et al. NF-κB activation in cardiac fibroblasts results in the recruitment of inflammatory Ly6Chi monocytes in pressure-overloaded hearts. *Sci. Signal.* **14**, eabe4932 (2021).
11. Amrute, J. M. et al. Targeting immune–fibroblast cell communication in heart failure. *Nature* **635**, 423–433 (2024).
12. Frangogiannis, N. G. Targeting macrophage–fibroblast interactions in the failing heart. *Nat. Rev. Cardiol.* **22**, 223–224 (2025).
13. Zhang, W. et al. Cardiac Fibroblasts Contribute to Myocardial Dysfunction in Mice with Sepsis: The Role of NLRP3 Inflammasome Activation. *PLoS ONE.* **9**, e107639 (2014).
14. Tomita, K. et al. Cardiac fibroblasts: contributory role in septic cardiac dysfunction. *J. Surg. Res.* **193**, 874–887 (2015).
15. Sato, R., Sanfilippo, F., Lanspa, M., Duggal, A. & Dugar, S. Sepsis-Induced Cardiomyopathy Mechanism, Prevalence, Assessment, Prognosis, and Management. *CHEST* **168**, 1383–1394 (2025).
16. Layland, J. et al. Protection against endotoxemia-induced contractile dysfunction in mice with cardiac-specific expression of slow skeletal troponin I. *FASEB J.* **19**, 1137–1139 (2005).
17. Wagner, S., Schürmann, S., Hein, S., Schüttler, J. & Friedrich, O. Septic cardiomyopathy in rat LPS-induced endotoxemia: relative contribution of cellular diastolic Ca2 + removal pathways, myofibrillar biomechanics properties and action of the cardiotonic drug levosimendan. *Basic. Res. Cardiol.* **110**, 50 (2015).
18. Dai, D. F. et al. Mitochondrial proteome remodelling in pressure overload-induced heart failure: the role of mitochondrial oxidative stress. *Cardiovasc. Res.* **93**, 79–88 (2012).
19. Schwarzer, M., Schrepper, A., Amorim, P. A., Osterholt, M. & Doenst, T. Pressure overload differentially affects respiratory capacity in interfibrillar and subsarcolemmal mitochondria. *Am. J. Physiol. -Hear Circ. Physiol.* **304**, H529–H537 (2013).
20. Hwang, H. V. et al. Transcriptomic and Functional Analyses of Mitochondrial Dysfunction in Pressure Overload-Induced Right Ventricular Failure. *J. Am. Hear. Assoc.* **10**, e017835 (2020).
21. Ranjbarvaziri, S. et al. Altered Cardiac Energetics and Mitochondrial Dysfunction in Hypertrophic Cardiomyopathy. *Circulation* **144**, 1714–1731 (2021).
22. Pan, P., Wang, X. & Liu, D. The potential mechanism of mitochondrial dysfunction in septic cardiomyopathy. *J. Int. Méd Res.* **46**, 2157–2169 (2018).
23. Stanzani, G., Duchen, M. R. & Singer, M. The role of mitochondria in sepsis-induced cardiomyopathy. *Biochim. Biophys. Acta (BBA) - Mol. Basis Dis.* **1865**, 759–773 (2019).
24. Robb, E. L. et al. Control of mitochondrial superoxide production by reverse electron transport at complex I. *J. Biol. Chem.* **293**, 9869–9879 (2018).
25. Rajendran, J. et al. Alternative oxidase-mediated respiration prevents lethal mitochondrial cardiomyopathy. *EMBO Mol. Med.* **11**, EMMM201809456 (2019).
26. Szibor, M. et al. Bioenergetic consequences from xenotopic expression of a tunicate AOX in mouse mitochondria: Switch from RET and ROS to FET. *Biochim. Biophys. Acta (BBA) - Bioenerg.* **1861**, 148137 (2020).
27. Szibor, M. et al. Respiratory chain signalling is essential for adaptive remodelling following cardiac ischaemia. *J. Cell. Mol. Med.* **24**, 3534–3548 (2020).
28. Viscomi, C., Moore, A. L., Zeviani, M. & Szibor, M. Xenotopic expression of alternative oxidase (AOX) to study mechanisms of mitochondrial disease. *Biochim. Biophys. Acta (BBA) - Bioenerg.* **1864**, 148947 (2023).
29. Szibor, M. et al. Broad AOX expression in a genetically tractable mouse model does not disturb normal physiology. *Dis. Model. Mech.* **10**, 163–171 (2017).
30. Giordano, L. et al. Alternative Oxidase Attenuates Cigarette Smoke–induced Lung Dysfunction and Tissue Damage. *Am. J. Respir Cell. Mol. Biol.* **60**, 515–522 (2019).
31. Saari, S. et al. Alternative respiratory chain enzymes: Therapeutic potential and possible pitfalls. *Biochim. Biophys. Acta (BBA) - Mol. Basis Dis.* **1865**, 854–866 (2019).
32. Sommer, N. et al. Bypassing mitochondrial complex III using alternative oxidase inhibits acute pulmonary oxygen sensing. *Sci. Adv.* **6**, eaba0694 (2020).
33. Zamora-Dorta, M. et al. Time-resolved mitochondrial screen identifies regulatory components of oxidative metabolism. *EMBO Rep.* **26**, 3045–3074 (2025).
34. Dassa, E. P. et al. Expression of the alternative oxidase complements cytochrome c oxidase deficiency in human cells. *EMBO Mol. Med.* **1**, 30–36 (2009).
35. Mills, E. L. et al. Succinate Dehydrogenase Supports Metabolic Repurposing of Mitochondria to Drive Inflammatory Macrophages. *Cell* **167**, 457–470e13 (2016).
36. Steinert, E. M. et al. Mitochondrial respiration is necessary for CD8 + T cell proliferation and cell fate. *Nat. Immunol.* **26**, 1267–1274 (2025).
37. Youle, R. J. & van der Bliek, A. M. Mitochondrial Fission, Fusion, and Stress. *Science* **337**, 1062–1065 (2012).
38. Holick, C. T. et al. Poly(2-ethyl-2-oxazoline) (POx) as Poly(ethylene glycol) (PEG)-Lipid Substitute for Lipid Nanoparticle Formulations. *Small* **21**, 2411354 (2025).
39. Li, X. P. et al. LPS induces activation of the TLR4 pathway in fibroblasts and promotes skin scar formation through collagen I and TGF-β in skin lesions. *Int. J. Clin. Exp. Pathol.* **12**, 2121–2129 (2019).
40. Arya, P., Sharma, V., Singh, P., Thapliyal, S. & Sharma, M. Bacterial endotoxin-lipopolysaccharide role in inflammatory diseases: An overview. *Iran. J. Basic. Méd Sci.* **28**, 553–564 (2025).
41. Espitia-Corredor, J. A. et al. Angiotensin II Triggers NLRP3 Inflammasome Activation by a Ca2 + Signaling-Dependent Pathway in Rat Cardiac Fibroblast Ang-II by a Ca2+-Dependent Mechanism Triggers NLRP3 Inflammasome in CF. *Inflammation* **45**, 2498–2512 (2022).
42. Kawaguchi, M. et al. Inflammasome Activation of Cardiac Fibroblasts Is Essential for Myocardial Ischemia/Reperfusion Injury. *Circulation* **123**, 594–604 (2011).
43. Epelman, S., Liu, P. P. & Mann, D. L. Role of innate and adaptive immune mechanisms in cardiac injury and repair. *Nat. Rev. Immunol.* **15**, 117–129 (2015).
44. Suetomi, T., Miyamoto, S. & Brown, J. H. Inflammation in nonischemic heart disease: initiation by cardiomyocyte CaMKII and NLRP3 inflammasome signaling. *Am. J. Physiol. -Hear Circ. Physiol.* **317**, H877–H890 (2019).
45. Campbell, S. E., Katwa, L. C. & Angiotensin II Stimulated Expression of Transforming Growth Factor-β1in Cardiac Fibroblasts and Myofibroblasts. *J. Mol. Cell. Cardiol.* **29**, 1947–1958 (1997).
46. Sano, M. et al. ERK and p38 MAPK, but not NF-κB, Are Critically Involved in Reactive Oxygen Species–Mediated Induction of IL-6 by Angiotensin II in Cardiac Fibroblasts. *Circ. Res.* **89**, 661–669 (2001).

47. Weber, K. T., Sun, Y., Bhattacharya, S. K., Ahokas, R. A. & Gerling, I. C. Myofibroblast-mediated mechanisms of pathological remodelling of the heart. *Nat. Rev. Cardiol.* **10**, 15–26 (2013).
48. Hartupee, J. & Mann, D. L. Role of inflammatory cells in fibroblast activation. *J. Mol. Cell. Cardiol.* **93**, 143–148 (2016).
49. Castro-Guerrero, N. A., Rodríguez-Zavala, J. S., Marín-Hernández, A., Rodríguez-Enríquez, S. & Moreno-Sánchez, R. Enhanced alternative oxidase and antioxidant enzymes under Cd2 + stress in Euglena. *J. Bioenerg Biomembr.* **40**, 227–235 (2008).
50. Perales-Clemente, E. et al. Restoration of electron transport without proton pumping in mammalian mitochondria. *Proc. Natl. Acad. Sci.* **105**, 18735–18739 (2008).
51. Billingham, L. K. et al. Mitochondrial electron transport chain is necessary for NLRP3 inflammasome activation. *Nat. Immunol.* **23**, 692–704 (2022).
52. Tarasenko, T. N. et al. Cytochrome c oxidase dependent respiration is essential for T cell activation, proliferation and memory formation. *Nat. Commun.* **16**, 10898 (2025).
53. Pinto, M. M. et al. The Warburg effect and mitochondrial oxidative phosphorylation: Friends or foes? *Biochim. Biophys. Acta (BBA) - Bioenerg.* **1864**, 148931 (2023).
54. Luengo, A. et al. Increased demand for NAD+ relative to ATP drives aerobic glycolysis. *Mol. Cell.* **81**, 691–707e6 (2021).
55. Vogler, B. T. L. et al. NanTex enables computational multiplexing and phenotyping of organelles across super-resolution modalities. *bioRxiv* 2025.09.16.676574 (2025). https://doi.org/10.1101/2025.09.16.676574
56. Giordano, L. et al. Alternative oxidase encoded by sequence-optimized and chemically-modified RNA transfected into mammalian cells is catalytically active. *Gene Ther.* **29**, 655–664 (2021).

Acknowledgements

The authors thank Judith Himmel (Dept. of Cardiothoracic Surgery, Jena University Hospital) and Katrin Hornung (Core Facility Cytometry, Institute of Immunology, Jena University Hospital) for excellent technical support. Furthermore, the authors would like to express their deep gratitude to Howard T. Jacobs (Tampere University) for providing critical materials and always insightful discussions. All authors are indebted to Ryan Titmas of Lucid Scientific (Boston, MA, USA) for providing the Resipher. MSZ was supported by intramural funds (LOM). MM received a scholarship from the Interdisciplinary Center for Clinical Research (IZKF). DD is principal investigator Germany's Excellence Strategy – EXC 2051 Balance of the Microverse – Project-ID 390713860. C.F. is supported by the Thüringer Aufbaubank (TAB, FGR 0060 KI-supER) and the DFG via the Collaborative Research Center PolyTarget (CRC 1278, project number 316213987, project B07). We thank the Microverse Imaging Center for providing microscope facility support. The Microverse Imaging Center is funded by the Deutsche Forschungsgemeinschaft (DFG, German Research Foundation) under Germany's Excellence Strategy – EXC 2051 – Project-ID 39071386 and project number 316213987 (CRC 1278, project Z01). The ELYRA 7 was funded by the Free State of Thuringia with grant number 2019 FGI 0003.

Author contributions

RAC, MSZ initiated and supervised the study. All authors participated in research design. LG generated immortalized mouse embryonic fibroblasts (iMEFs). MM, CS conducted cell culture experiments, the measurements of oxygen consumption rates (OCRs), and gene and protein expression analyses. LH, CF performed immunocytochemistry and super-resolution imaging. JV and RAC provided useful suggestions for article writing. All authors have read and agreed to the submitted version of the manuscript.

Funding

Open Access funding enabled and organized by Projekt DEAL. MSZ was supported by intramural funds (LOM) from the Jena University Hospital. MM received a scholarship from the Interdisciplinary Center for Clinical Research (IZKF). DD is principal investigator Germany's Excellence Strategy – EXC 2051 Balance of the Microverse – Project-ID 390713860. CF is supported by the Thüringer Aufbaubank (TAB, FGR 0060 KI-supER) and the DFG via the Collaborative Research Center PolyTarget (CRC 1278, project number 316213987, project B07). The authors thank the Microverse Imaging Center for providing microscope facility support. The Microverse Imaging Center is funded by the Deutsche Forschungsgemeinschaft (DFG, German Research Foundation) under Germany's Excellence Strategy – EXC 2051 – Project-ID 39071386 and project number 316213987 (CRC 1278, project Z01). The ELYRA 7 was funded by the Free State of Thuringia with grant number 2019 FGI 0003.

Declarations

Competing interests

MSZ declares himself a co-founder of a startup company to develop AOX therapeutics. DD was a consultant of Johnson & Johnson and received funding by Affimed. All other authors have no competing interests related to this work.

Additional information

Supplementary Information The online version contains supplementary material available at https://doi.org/10.1038/s41598-026-61303-1.

Correspondence and requests for materials should be addressed to M.S.

Reprints and permissions information is available at www.nature.com/reprints.

Publisher's note Springer Nature remains neutral with regard to jurisdictional claims in published maps and institutional affiliations.

Open Access This article is licensed under a Creative Commons Attribution 4.0 International License, which permits use, sharing, adaptation, distribution and reproduction in any medium or format, as long as you give appropriate credit to the original author(s) and the source, provide a link to the Creative Commons licence, and indicate if changes were made. The images or other third party material in this article are included in the article's Creative Commons licence, unless indicated otherwise in a credit line to the material. If material is not included in the article's Creative Commons licence and your intended use is not permitted by statutory regulation or exceeds the permitted use, you will need to obtain permission directly from the copyright holder. To view a copy of this licence, visit http://creativecommons.org/licenses/by/4.0/.

© The Author(s) 2026